International Forum on Aeroelasticity and Structural Dynamics
IFASD 2017
25-28 June 2017 Como, Italy

NUMERICAL INVESTIGATION OF VIRTUAL CONTROL SURFACES FOR AEROELASTIC CONTROL ON COMPRESSOR BLADES

Valentina Motta[1], **Leonie Malzacher**[1], **and Dieter Peitsch**[1]

[1]Institute of Aeronautics and Astronautics, Chair of Aero engines
Technische Universität Berlin
Marchstraße 12–14, 10587 Berlin, Germany
valentina.motta@tu-berlin.de

Keywords: linear compressor cascade, active flutter control, virtual surfaces, plasma actuators

Abstract: Virtual control surfaces are assessed numerically as a means to enhance the aeroelastic response of a compressor cascade. Virtual surfaces are realized with plasma actuators placed on the pressure and on the suction side of the blade trailing edge. Advantages of plasma actuators over mechanical control surfaces are the absence of failure risks when operating under centrifugal and temperature fields typical of compressors used in aero engines. The plasma-induced flow is meant to be against the direction of the freestream. This allows for generating controlled recirculating flow areas and in turn modifying the effective blade camber and enlarging the actual chord. Computational fluid dynamic analyses with the blades at constant angle of attack show that the effects of pressure side actuation on flow field, pressure distribution and integral loads are comparable to those of flap-like devices. On the contrary suction side actuation yields effects which are analogous to those of wing spoilers. Traveling wave simulations for the torsion mode show that properly triggering an alternate pressure/suction side actuation during the pitching cycle improves significantly the blade aeroelastic stability. At the same time an effective reduction in the peaks of the oscillating airloads is achieved, with potential benefits for the alleviation of fatigue.

1 Introduction

The demand for lighter and more efficient aero engines has remarkably grown during the last few years. To address this issues modern compressors have been conceived with increasingly larger pressure ratios per stage. Natural consequences of these solutions are an aggressive blade loading and high flutter sensitivity, especially for long and slim blades. Blade design approaches aiming specifically at improving the aerostructural stability have been proposed e.g. in Refs. [1, 2]. Also the aerodynamic performance is much affected on such highly loaded blades. Indeed larger pressure gradients over the blade suction surface may anticipate the stall onset, therefore degrading the overall compressor performance. Diverse active flow control solutions have been proposed to optimize the aerodynamic performance of heavily loaded blades. Flow blowing trough side wall actuators has been widely studied as a potential means to suppress three dimensional secondary flow phenomena, and to reduce separated flow areas on heavily loaded blades [3–5]. Besides blowing, blade morphing mechanisms have been widely investigated to assess their capabilities in enhancing the aerodynamic response of highly loaded

compressor and turbine blades. Solutions like blades with adjustable angle of attack, movable leading edge, Gurney flaps, and adaptive camber – usually driven by piezo-actuators or shape memory alloys – have been proved to have a significant affection on the developed airloads, see Refs. [6–9]. Large interest has been latterly addressed towards plasma actuation. The suitability of plasma actuators stems from their lightness and their non-intrusiveness into the flow field. Additionally the absence of mechanical parts avoids the risk of structural and operational failures, likely to occur under high centrifugal loads typical of aero engines. Several numerical and experimental assessments have been carried out to investigate the affection of plasma actuators on the aerodynamic performance of heavily loaded blades. It has been proved that appropriate locations and actuation strengths allow for suppressing spike stall inception [10], reducing pressure losses [11] and controlling corner stall separation [12].

Mechanical trailing edge control surfaces deflected harmonically have been proved to be an effective means to reduce detrimental vibratory loads on helicopter rotors, due to their twofold operation. Indeed upward deflections of these devices yield effects comparable to those achievable with fixed wing spoilers, i.e. an alleviation of the sectional loading. On the other hand downward deflections provide an augmentation of the blade loading. Properly phased harmonic deflection of these surfaces – alternately upward and downward – allows to smooth the peaks of unsteady airloads arising from the blade oscillations. As a result blade vibration can be minimized. Within this framework, Refs. [**?**, **?**, **?**, **?**, **?**, 13] investigate individually controlled trailing edge flaps to reduce vibratory loads at frequencies which are multiple of the rotor angular velocity. The effectiveness of these devices – when proper amplitude, frequency and phase of actuation are used – is demonstrated numerically and experimentally. Refs. [**?**, **?**, 14] study variously shaped microflaps for vibration reduction on rotorcraft. The multidisciplinary analyses carried out in these works show that these devices – extracted and retracted harmonically – can effectively withdraw dynamic loads at different frequencies and in turn manipulate the corresponding blade modes. The works of Refs. [15–19] present computational fluid dynamic and aeroelastic assessments of a L-shaped Gurney flap installed on the trailing edge of helicopter blades. An optimization procedure is used to tune the parameters for the harmonic actuation of this device in order to minimize the blade root vibratory loads. It is shown that the blade root vertical force and bending moment at frequencies between 2/rev and 5/rev can be reduced by almost 100%.

A twofold operating control solution, capable to both increase and decrease loading, is particularly desirable also for highly loaded blades. This would allow for manipulating effectively self induced vibration and for enlarging flutter boundaries. However mechanical devices are likely to undergo failures when operating under centrifugal and temperature fields encountered on aero engine compressors. It seems a promising approach to reproduce the flow field effects provided by the mentioned mechanical devices with actuators which are more suitable for turbomachinery applications. Among the possible solutions, plasma actuation is considered as the most appropriate for this purpose. Other means of flow control such as jet blowing/suction, piezoelectric morphing and acoustic excitation have been taken under consideration, but then discarded. Potential drawbacks of flow blowing are the following: i) blade holes are intrusive in the flow field; ii) the blowing frequency and intensity is not trivial to control; iii) the bandwidth is lower relative to plasma or piezo-actuators. Possible limitations of piezo-electric actuation are the following: i) a mechanical chain for displacement amplification may be required, with possible risks of operational or structural failure; ii) the operating temperature range may not be suitable for compressor applications; iii) fragility and fatigue phenomena affect severely the operational reliability. Potential drawbacks of acoustic excitation may be: i) internal (on-blade)

sound sources require blade holes that may be intrusive in the flow field and detrimental for the structural integrity; ii) external sources require hardware for loud speakers, not trivial to implement on the engine casing; iii) the control is ineffective when trailing edge separation occurs.

This work presents a numerical assessment of plasma actuators employed to reproduce the effects of mechanical control surfaces, deflected steadily and harmonically, both upward and downward. It is shown that plasma can indeed operate as a virtual control surface and can manipulate both vibration and aeroelastic stability of a compressor cascade. Plasma actuators are modeled on the pressure and on the suction side at the blade trailing edge. Plasma actuation is here expected to develop vortical structures and recirculating flow areas comparable to those generated by mechanical control surfaces. With this aim the plasma induced flow is conceived to be opposite relative to the freestream direction [20, 21]. First numerical computations are performed on the clean configuration and compared to experimental data obtained on the same cascade in the wind tunnel facility of the Chair of Aero Engines at Technische Universität (TU) Berlin [22]. Both constant angle of attack and traveling wave simulations for the pitch mode are carried out. In this case all the blades oscillate at the same amplitude and frequency but with different phasing – referred to as inter blade phase angle (IBPA). The numerical results obtained with traveling wave mode simulations are also compared to the measurements of Refs. [**?**, 23]. Subsequently constant angle of attack simulations are performed with plasma actuators modeled either on the pressure or on the suction side of the three central blades. It is shown that indeed pressure/suction actuation can alter the blade local and resulting loading in a way that is comparable to the effects induced by wing flaps and spoilers, respectively. Traveling wave mode simulations are then performed with alternate pressure/suction side actuation. Namely pressure side actuation is triggered during the downstroke phase of the pitching cycle – i.e. nose down. On the other hand suction side actuation is triggered during the upstroke phase of the pitching cycle – i.e. nose up. This operation is also consistent with the remarks of [24], in which the effects on the aerodynamic work of the L-tab of [15–19], kept deflected upward of deployed downward, were measured in dynamic stall conditions. It is shown that the proposed unsteady plasma actuation allows for increasing the blade aeroelastic stability – in terms of aerodynamic work – as well as for reducing the oscillations of unsteady airloads, especially the lift. The manuscript is articulated as follows. Section 2 deals with the numerical model for the computational fluid dynamic (CFD) assessments carried out in this work. The flow solver, the computational geometry and the numerical modeling of plasma actuators are illustrated in detail. The results of constant angle of attack and traveling wave mode simulations obtained on the clean cascade are then presented and compared with experimental and literature results. Section 3 discusses the results obtained with CFD computations at constant angle of attack with plasma actuation either on the pressure or on the suction side. The effects of plasma on pressure, integral airloads and flow field obtained at angles of attack α between 0 and 12 degrees are illustrated. Section 4 describes the results of traveling wave mode simulations with alternate pressure/suction side actuation. The effects on flow field, unsteady airloads, and aerodynamic work are discussed in detail. Section 5 provides concluding remarks to the present work.

2 Numerical model

Computational fluid dynamic analyses are carried out on a seven blade cascade, reproducing the span-wise uniform experimental model for wind tunnel aeroelastic assessments in use at the Chair of Aero Engines of TU Berlin [22]. Indeed adopting the same geometry of the experimental model allows to rapidly check the reliability of the performed numerical results, at least for the clean cascade. The blade section is an airfoil of the NACA 65 series featuring a chord length of $c = 0.15$ m. The pitch to chord ratio is equal to 0.75 and the stagger angle corresponds to 43 degrees. A sketch of the numerical geometry is shown in figure 1. Experimental tests performed on this cascade have shown negligible three-dimensional effects in the flow behaviour, at least for the conditions of interest here, see [22]. Additionally plasma actuators are meant to cover the entire blade span, yielding as a first approximation uniform effects from the root to the tip. Therefore two-dimensional numerical simulations are performed throughout this work.

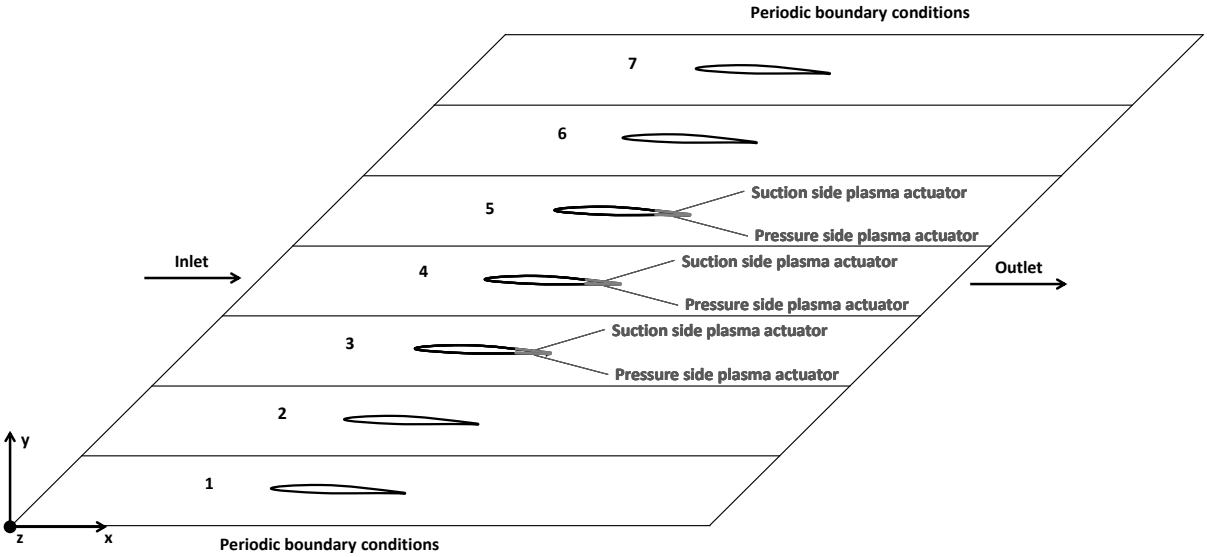

Figure 1: Schematic of the computational geometry for the compressor cascade.

The computational mesh consists of a multi-block structured grid composed of 550949 elements. The airfoil edge features 410 elements, distributed in order to enhance the resolution on the leading and on the trailing edge, as well as on the region where plasma is modeled. The height of the first cell on the solid wall is set to get $y^+ = 1$ for a Reynolds number $\mathrm{Re} \sim 10^5$ – being this latter based on the blade chord and on the freestream velocity. The grid extends approximately two chords both upstream the leading edge and downstream the trailing edge. A detail of the computational grid around the blade, together with a blow up in the traling edge is shown in figure 2. Tip and hub gaps are not modeled within the computational domain.

The freestream velocity is imposed as at the inlet, whereas a pressure of 101325 Pa is defined at the outlet. Periodic boundary conditions are used at the top and at the bottom of the computational domain. The velocity is set to zero on the blade edges, as viscous computations are carried out.

Numerical computations are carried out with the flow solver Ansys CFX. It is a finite volume solver capable to perform both compressible and incompressible simulations. A high resolution scheme is used for the advection terms of the Navier-Stokes equations, and a second order

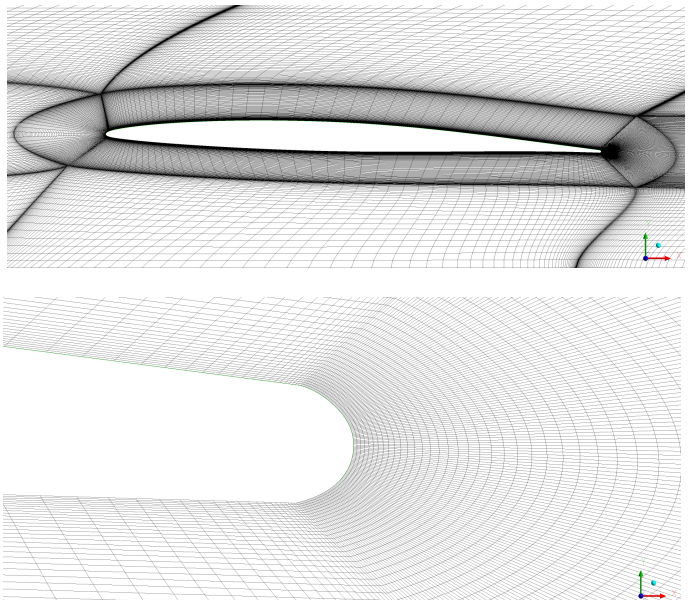

Figure 2: Detail of the computational grid around the blade (top), and blowing up on the trailing edge (bottom).

backward scheme is employed for the transient terms. The flow is assumed as fully turbulent, and the the SST k-ω model is used to close the system of Reynolds-Averaged Navier-Stokes equations employed for the present assessments.

Figure 3 shows a schematic of a single dielectric barrier discharge plasma actuator. Two electrodes are separated by a dielectric barrier material. One electrode is exposed to air, i.e. on the aerodynamic surface, and one is grounded within the dielectric material, inside the blade internal volume.

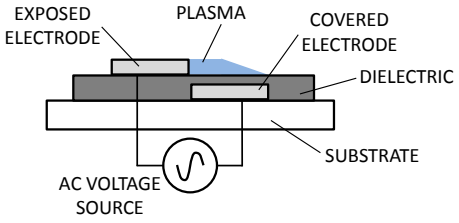

Figure 3: Schematic of a plasma actuator.

When an alternate current voltage is applied between the electrodes, a plasma discharge is initiated. As a consequence air is locally ionized in the area close to the electrodes and the flow momentum can be manipulated. Therefore the essential effect of plasma actuators is to add momentum into the flow field and in turn to modify the local velocity profile, see e.g. Ref. [25]. A source term is here added to the momentum equations in order to model the plasma induced flow. Specifically a uniform force per unit volume is applied over a limited region always bounded on one side by the airfoil wall. Notice that this approach is consistent with that of Refs. [26–28]. The plasma is here meant to act on a completely attached flow at Re $\sim 10^5$, with x component opposite to the main freestream direction – the y component is set in order to keep the plasma always tangent to the airfoil. Therefore the body force has to be larger compared to classical low Re applications. Consistently with the assessments of Ref. [12] and with the experiments of Ref. [29], a uniform force per unit span ranging between 225 and 450 mN/m is

used in this work. Notice that this approach is employed also in Refs. [26–28, 30]. The plasma region is modeled as a quadrangle 0.1 mm thick and 10 mm wide, see figure 4. Notice that these sizes are the same used in Refs. [10, 26] and representative of the experimental models of Refs. [12,21,31]. Assessments are performed with plasma actuators located on the trailing edge, both on the pressure and on the suction side, see again figure 4. For alternate pressure/suction side actuations, employed during traveling wave mode simulations, smoothing functions are applied to the body force to avoid step-like changes in the blade loading. It's worth remarking that the main concern of this work is to assess how plasma actuators can potentially act on aeroelastic stability and vibration of a cascade. The development of a more accurate model of the plasma induced flow field, is planned as an outlook for the present activities.

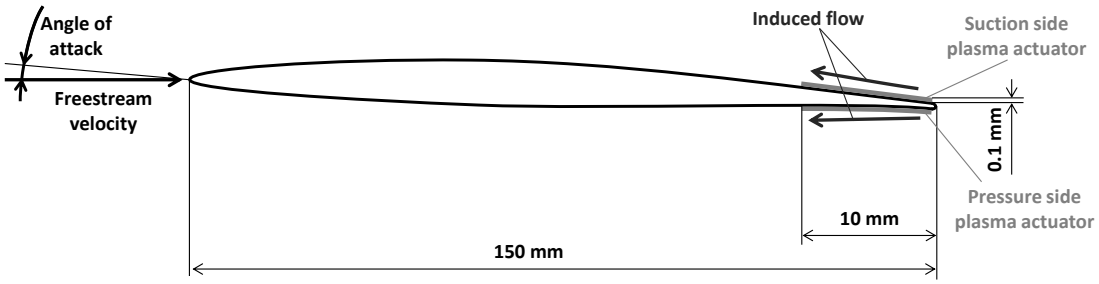

Figure 4: Sketch of the blade section with the modeling of plasma actuators.

A comparison between the pressure distribution computed on the central blade of the cascade and the experimental counterpart is depicted in figure 5. The measurements have been performed on the test rig of the Chair of Aero Engines. The angle of attack of the blades corresponds to 2 degrees, whereas the imposed freestream velocity U_∞ is equal to 34.36 m/s, yielding a Reynolds number of $\sim$ 350000 and a Mach number of $\sim$ 0.06. The numerical and experimental data exhibit a very good agreement, including the leading edge and trailing edge regions. This matching confirms also that the periodic flow conditions applied at the top and at the bottom of the cascade do not induce undesired reflection effects, at least on the considered central blades of the cascade.

Figure 6 shows the results of time-resolved traveling wave mode simulations performed on the clean cascade and compared to the experimental counterpart, as well as to the measured data of Carta [23] and Sachs [**?**]. Namely the real and imaginary part of unsteady pressure are computed separately for the pressure and for the suction side of the central blade. The real part of the suction side is then subtracted to the counterpart of the pressure side, to get the displayed quantity $\Delta_{\mathrm{C_P}}$. The same procedure is adopted for the imaginary part. The numerical results are found in good agreement with the experimental and literature data, in terms of both real and imaginary part. Light differences are encountered just downstream the leading edge, where however all the plotted data are remarkably scattered. The comparison is performed for the blades oscillating at frequency of 5.25 Hz, corresponding to a reduced frequency $\mathrm{k} = 2\pi\mathrm{fc}/\mathrm{U}_\infty = 0.1440$ – with the same inlet velocity used for the comparisons at constant angle of attack. The IBPA is equal to 0 degrees.

Time-resolved simulations are carried out with the blades at constant angle of attack, to check the steadyness in the mean of the plasma induced effects. This is meant to prove the reliability of the steady-state results achieved at constant angle of attack which are presented in the fol-

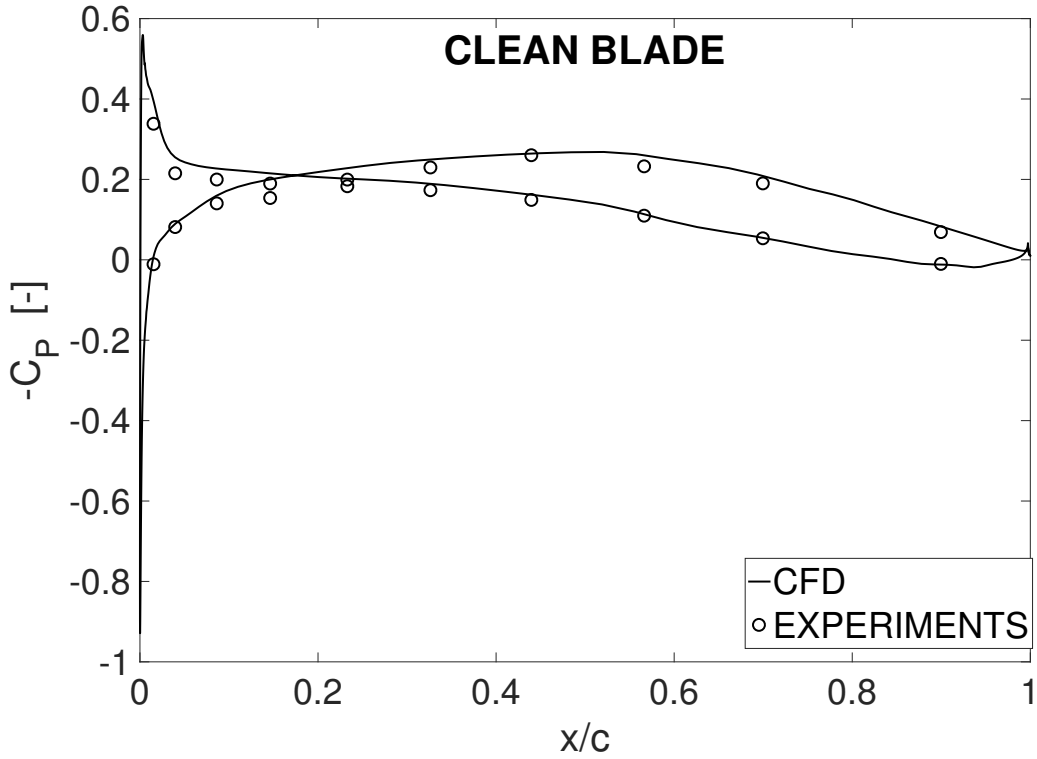

Figure 5: Pressure coefficient distribution on the cascade central blade. Experiments and CFD on the clean configuration; Re $\sim 3 \times 10^5$, $\alpha = 2$ deg.

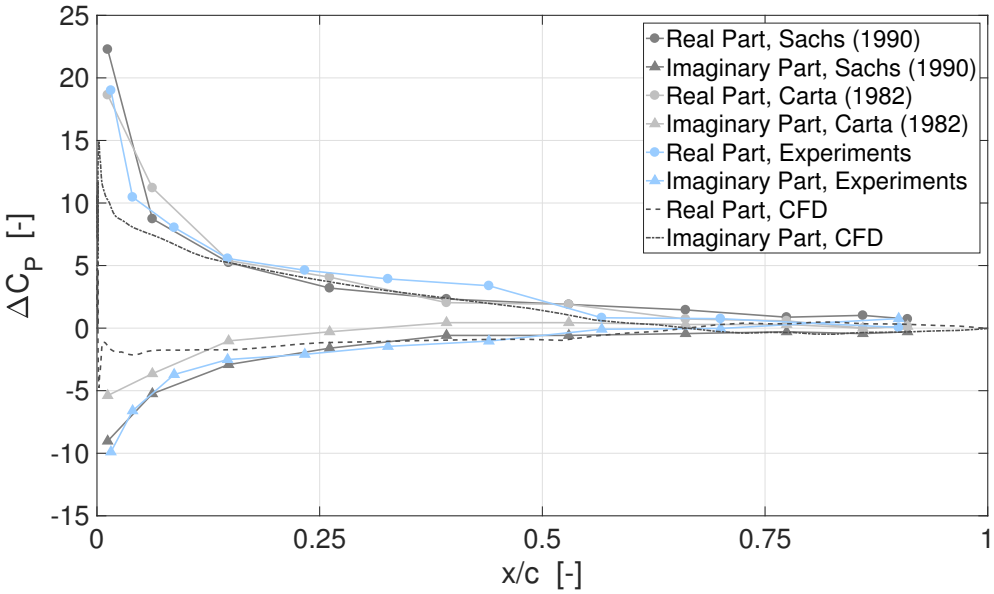

Figure 6: Real and imaginary part of unsteady pressure distribution. Experiments and CFD on the clean configuration; Re $\sim 3 \times 10^5$; IBPA = 0 deg.; $\alpha = 2 + \sin 2\pi \mathrm{f\,t} + \mathrm{IBPA}\pi/180$ degrees; f $= 5.25$ Hz; t: time.

lowing. Figure 7 shows the time history of the lift $\mathrm{C_l}$, drag $\mathrm{C_d}$ and mid-chord moment $\mathrm{C_{m_{c/2}}}$ coefficients at $\alpha = 2$ degrees and Re $\sim 3 \times 10^5$. The time step for the unsteady computations is 1.6685×10^{-4} s. Each of the three airloads converges to a constant value after a maximum of ~ 0.015 s, for the clean configuration as well as for the pressure/suction side plasma equipped configuration. Therefore steady state computations are suitable to investigate the mean effects

of plasma actuation when the blades are kept at constant angle of attack.

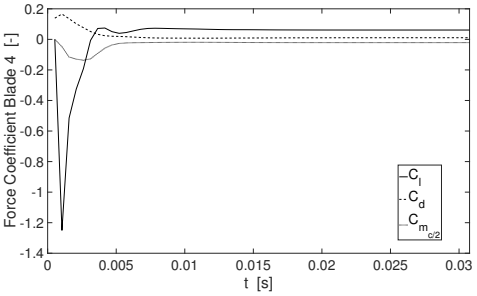

(a) Clean blade

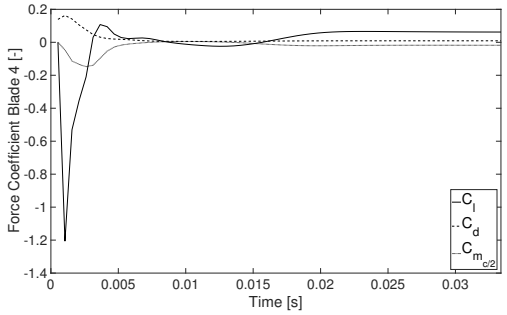

(b) Pressure side actuation

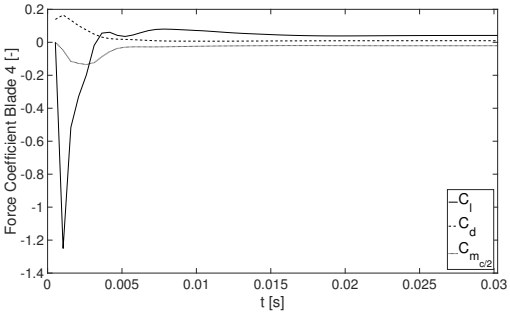

(c) Suction side actuation

Figure 7: Time history of unsteady lift C_l, drag C_d and mid-chord moment coefficient $C_{m_{c/2}}$ at constant angle of attack of 2 degrees; Re $\sim 3 \times 10^5$; uniform constant body force at 300 mN/m.

3 Assessments at constant angle of attack

Numerical simulations are performed at constant angle of attack to characterize the affection of pressure and suction side plasma on mean flow field and loads. A body force of 300 mN/m is used to model both the pressure and the suction side plasma actuators. The Reynolds number for the simulations discussed in this section is 341076. Angle of attacks ranging between 2 and 12 degrees are considered. For brevity purposes results are reported for the central blade only. The same results are obtained on the other plasma equipped blades.

Figure 8 shows the velocity magnitude normalized over the freestream velocity, and the vorticity, this latter made dimensionless by the ratio between the chord and the freestream velocity. These plots result from numerical simulations carried out at angle of attack of 2 degrees. A detail of the trailing edge is displayed for the clean blade and for the configurations with pressure and suction side plasma, respectively. Both actuations lead to the development of low speed recirculating flow areas, with a consequent modification of local and resulting loads. In particular pressure side plasma leads to the development of steady-in-the-mean vortical structures that shift the application point of the Kutta condition downstream the physical trailing edge. This is approximately equivalent to employing a longer and more cambered airfoil, relative to the baseline section. Therefore lift augmentations are expected to be direct consequence of this phenomenon. A modification in the effective camber is induced by suction side actuation as well. In this case the induced camber modification is opposite to that provided by pressure side plasma. That is the resulting actual camber will shift the zero-lift angle to a positive value.

Accordingly the lift curve is expected to undergo a downward vertical shift with respect to the clean blade. As expected the wake results thicker compared to the clean blade counterpart. However it will be shown that no significant drag increases are encountered on the actuated configurations. The pressure coefficients computed with the clean configuration, as well as with pressure and suction side actuation, are displayed in figure 9. The behaviour of the load distribution is consistent with the flow fields of figure 8. Namely both the actuations modify the pressure distribution along the entire chord, up to the leading edge. In particular the area covered by the $-C_P$ curve is enlarged with pressure side actuation and reduced with suction side actuation. Therefore remarkable modifications are expected to be observed on the resulting loads, especially in terms of resulting lift coefficient. It's worth remarking that these results are in qualitative agreement with the assessments of Refs. [15–19], where the same effects were obtained with a mechanical L-tab deflected downward or upward, installed on a helicopter blade section. A similar behaviour of pressure coefficient is encountered also in Ref. [**?**], where the effects of downward and upward displacements of the morphing trailing edge on a wind turbine blade are assessed. Additionally the computed flow fields are qualitatively consistent with the measurements of Feng et al. [20] on a low speed fixed wing section with pressure side plasma actuators featuring an induced flow opposite to the freestream direction.

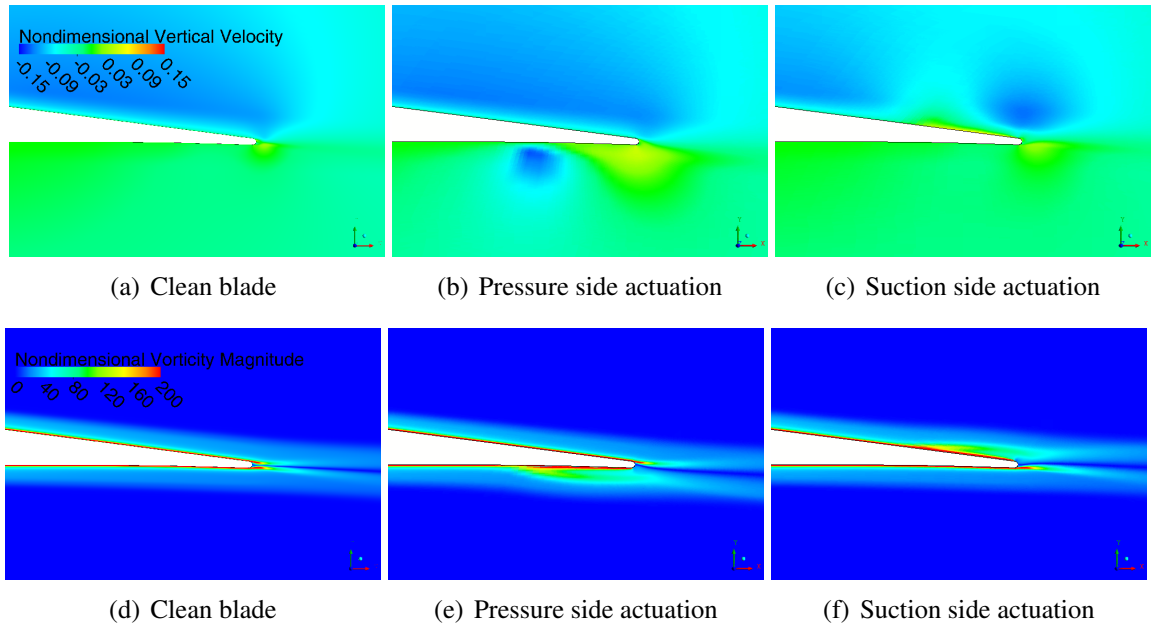

(a) Clean blade (b) Pressure side actuation (c) Suction side actuation

(d) Clean blade (e) Pressure side actuation (f) Suction side actuation

Figure 8: Top: trailing edge detail of vertical (y-parallel) velocity magnitude normalized by the freestream velocity. Bottom: z-vorticity magnitude normalized by the chord/freestream velocity ratio, for the clean cascade, and with pressure/suction side actuation. Re $\sim 3 \times 10^5$, $\alpha = 2$ degrees.

Figure 10 shows the lift, the drag and the quarter-chord moment coefficients versus the blade angle of attack, computed for the clean blade and with the pressure or suction side actuation. The Reynolds number is Re = 341076. As anticipated, actuation yields a modification of the effective camber – opposite for pressure and suction plasma – and a chord-wise shift of the Kutta condition downstream the trailing edge. Actually the influence of the neighbouring blades yields per se a modification in the effective camber. Indeed at $\alpha = 0$ deg. the computed lift coefficient is larger than 0. Concurrently the quarter-chord moment coefficient is no longer unchanged relative to the angle of attack because the camber modification effects cause a chord-wise shift of the aerodynamic centre. Pressure side actuation provides an increase in lift relative to the clean blade. The lift curve exhibits a shift upward, so that at equal angle of attack the lift

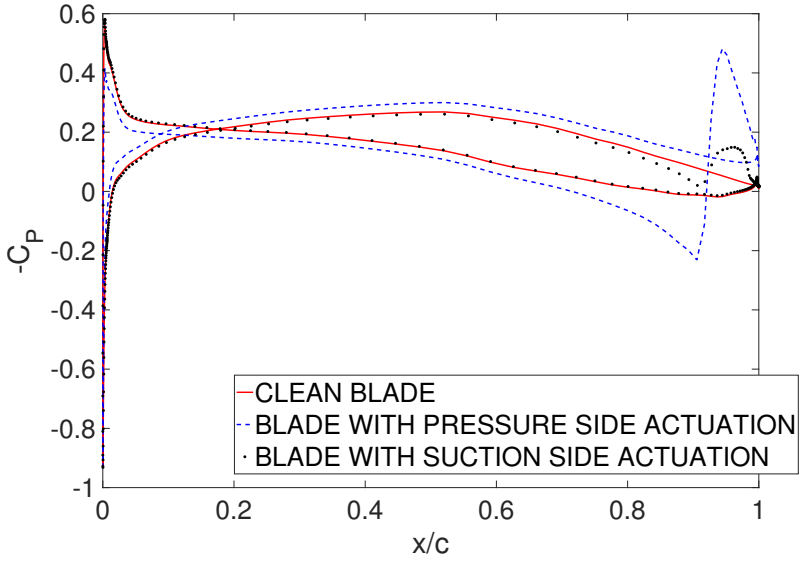

Figure 9: Pressure coefficient distribution. Computations on the clean blade and with pressure/suction side actuation. Re $\sim 3 \times 10^5$, $\alpha = 2$ degrees.

generated is larger. This behaviour is indeed consistent with the effects achieved on fixed and rotary wings equipped with trailing edge flap-like devices [**?**, 18, 32]. The zero-lift angle of attack is also shifted to a negative value. Consistently with Refs. [18, 33] no significant drag rises are encountered. The nose-down positive moment coefficient is increased with pressure side actuation, therefore enhancing the blade torsional stability. Opposite effects are observed with suction side actuation. That is the lift curve is shifted downward, consistently with the behaviour of wing spoilers. The zero-lift angle is shifted to a positive values. Also in this case there are not significant rises in drag, again in agreement with [18, 33]. Actually a drag reduction is encountered at $\alpha = 12$ degrees. This is probably due to the incipient trailing edge separation occurring at this angle of attack. Because suction side actuation reduces the effective angle of attack the onset of separation, together with the concurrent increase in drag, is shifted toward larger values of α. Only a light decrease in terms of quarter chord moment coefficient is achieved with suction side actuation. This is particularly promising, because – at least in terms of steady state effects – suction side actuation does not appear as detrimental for the torsional stability. In general both pressure and suction side plasma provide percent lift modifications quantitatively comparable to those of Refs. [**?**, 15–19] achieved with a mechanical L-shaped Gurney flap. The same can be said in terms of drag coefficient. It's worth remarking that also the behaviour of pitching moment according to pressure/suction side actuation is consistent with the results of several works in literature dealing with mechanical trailing edge control surfaces, e.g. Refs. [18, 24, 32].

Overall pressure side actuation provides larger absolute gains of lift and moment compared to suction side actuation. This is probably due to the higher velocity gradients encountered on the suction side. As a consequence a larger body force should be applied on the suction side, to obtain comparable effects on the resulting forces. On the basis of these results, the traveling wave mode simulations discussed in the following are performed with a larger body force on the suction side and a smaller one on the pressure side.

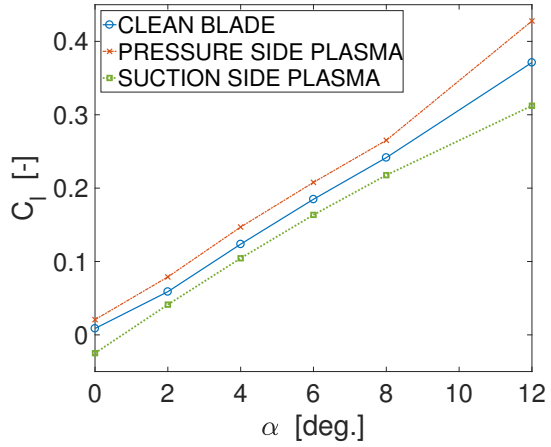

(a) Clean blade

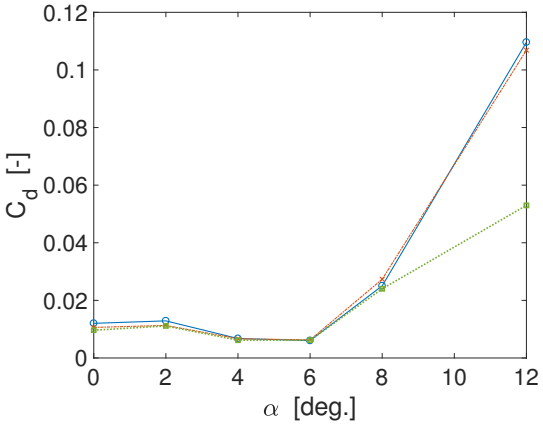

(b) Pressure side actuation

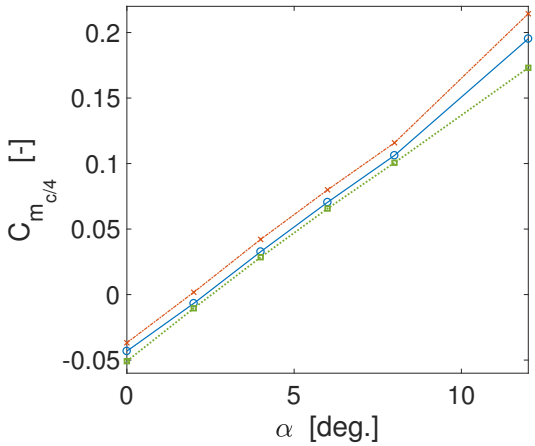

(c) Suction side actuation

Figure 10: Steady force coefficients versus the angle of attack for the clean central blade, together with the pressure or suction side actuated counterpart; Re $\sim 3 \times 10^5$.

4 Assessments with traveling wave mode simulations

Traveling wave mode simulations are performed for harmonic pitch oscillations of the blades with IBPAs between -180 and 180 degrees. Here positive IBPA indicates a wave traveling from the pressure to the suction side. The freestream velocity is set to 19.65 m/s, yielding a Reynolds number of 195057. The oscillation frequency is set to 19.17 Hz, with a resulting k of 0.9195. The mean angle of attack is set to 2 deg. and the oscillation amplitude is set to 1 degree. The resulting oscillation law for the i^{th} blade writes: $\alpha(\mathrm{t}) = 2 + \sin(2\pi \mathrm{f}\, \mathrm{t} + \mathrm{i} \times \mathrm{IBPA})$ degrees. These specific values of Reynolds number, reduced frequency, mean angle of attack and oscillation amplitude are used because experiments on the same cascade detected the occurring of flutter at these conditions, specifically for IBPA = -51.43 degrees [34]. As a consequence these conditions are regarded as particularly appropriate for assessing the effects of plasma on the blade aeroelastic stability. An alternate pressure/suction side actuation, defined according to the time derivative of the blade motion law, is imposed. Suction side actuation is triggered during the upstroke phase of the pitching cycle. On the contrary suction side actuation is switched on during the downstroke phase of the pitching cycle. Consistently with the differences in the ve-

locity gradients at the trailing edge on the pressure and on the suction side, the body forces are set to 450 mN/m on the upper side and to 225 mN/m on the lower side. It's worth recalling that smoothing functions are applied to the body force at the beginning and at the end of the actuator operating cycle. This avoids undesired discontinuities in the blade loading when switching from pressure to suction side actuation and vice versa. Figure 11 shows trailing edge details of the velocity magnitude field during an oscillation cycle. The velocity is made dimensionless with the freestream velocity. The central blade of the cascade is displayed. Pressure side actuation yields the desired recirculating flow areas during the downstroke phases, with expected increase in the blade loading relative to the clean counterpart. The opposite occurs during the upstroke phase. Notice that the recirculating flow area achieved on the suction side is slightly larger compared to the pressure side counterpart. This is indeed consistent with the employment of a larger body force on the suction side, aiming to get the same effectiveness on the flow momentum. Indeed, as anticipated, the velocity gradient on the trailing edge suction side is larger than on the pressure side counterpart. Further tuning of the pressure/suction side body forces would allow to get an almost identically sized recirculating flow areas on the pressure and on the suction side. The case of IBPA = -51.43 deg. has been plotted, because it corresponds to the fluttering condition detected experimentally mentioned above [34].

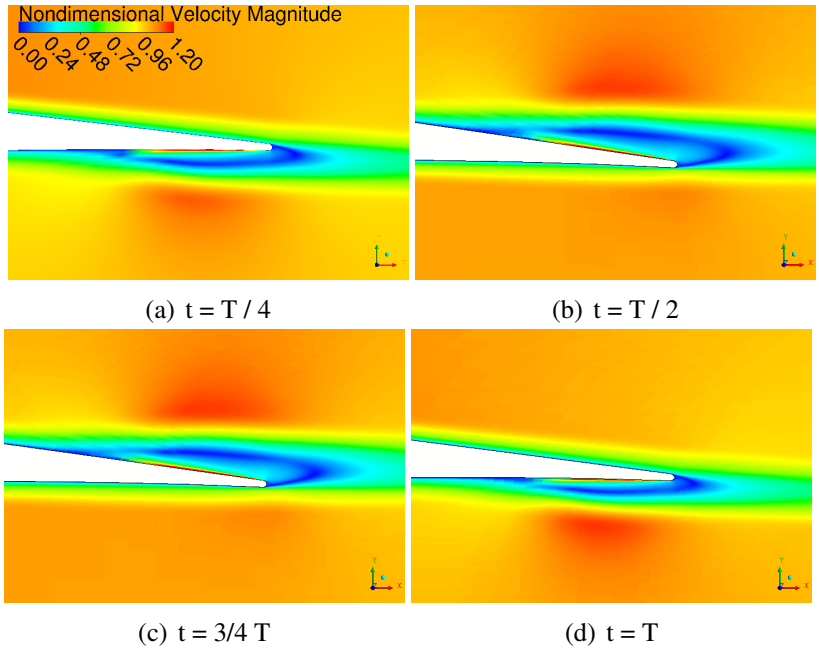

(a) t = T / 4 (b) t = T / 2

(c) t = 3/4 T (d) t = T

Figure 11: Trailing edge detail of velocity magnitude, normalized by the freestream velocity, over the oscillation cycle; plasma actuation on; Re ∼195000; IBPA = -51.43 deg.; $\alpha = 2 + \sin 2\pi \mathrm{f}\, \mathrm{t} + 4 \times \mathrm{IBPA}\pi/180$ deg.; $\mathrm{f} = 19.17$ Hz, $\mathrm{T} = 1/\mathrm{f}$.

The aerodynamic work is used as reference parameter to assess the aerostructural stability of the cascade. This quantity defines the energy exchanged between the blade and the flow. When the flow transfers energy to the blade, then the section is unstable and flutter can occur. On the contrary, when the blades feed the flow with energy, then the sectional oscillations are damped out and the system is stable. The aerodynamic work results from integrating the scalar product between the pressure fluctuations $\tilde{p}$ and the velocity locally normal to the airfoil over the blade surface ℓ:

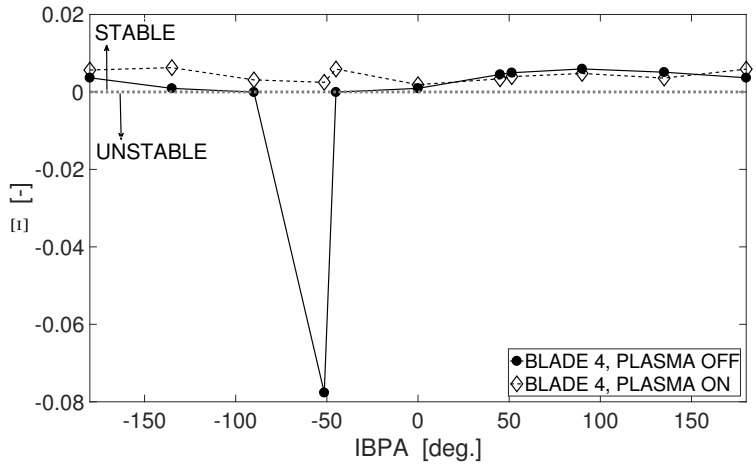

Figure 12: Aerodynamic damping coefficient versus IBPA for the clean and the plasma equipped configuration. The dashed grey line tracks the stability threshold; Re $\sim$195000; $\alpha = 2 + \sin 2\pi \mathrm{f}\, \mathrm{t} + 4 \times \mathrm{IBPA}\pi/180$ degrees; $\mathrm{f} = 19.17$ Hz, $\mathrm{T} = 1/\mathrm{f}$.

$$W = \int_{\ell} \tilde{p}\, \boldsymbol{u} \times \hat{\mathbf{n}}\, d\ell\,, \tag{1}$$

The aerodynamic work depends only on the local pressure and displacement velocity of the blade and can be directly issued from CFD computations [35–40]. The aerodynamic damping coefficient – the non dimensional counterpart of the aerodynamic work – is expressed as [1]:

$$\Xi = -\frac{W}{\pi \mathrm{q} \mathrm{c}^2 \bar{\alpha}^2}, \tag{2}$$

being $\mathrm{q} = 1/2\rho \mathrm{U}_{\infty}^2$, the dynamic pressure, ρ the density and $\bar{\alpha}^2$ the amplitude of the pitching oscillations. Negative values of Ξ indicate that the blade is unstable and flutter can occur. For positive values of Ξ the blade is stable. Figure 12 depicts the damping coefficient versus the IBPA for the clean and for the plasma-equipped cascade. Only the results on central blade are reported here, though the same behaviour is observed for each of the three plasma equipped sections. Consistently with the measurements of [34] an instability peak is encountered at IBPA = -51.43 degrees. The actuation allows to withdraw completely this peak and the corresponding aerodynamic damping is shifted back to a positive value. This is a very promising result and plasma actuation shows great potential in preventing the occurring of dangerous aeroelastic stabilities. Additionally an effective stabilizing effect is obtained at each of the simulated negative IBPAs, being all of these very close to the instability threshold for clean cascade. Indeed the damping coefficient achieved with plasma actuation is remarkably shifted upward compared to the clean blade counterpart. At positive IBPAs the clean cascade is stable. For a few positive IBPAs actuation yields a light decrease of the damping coefficient, but in any case the observed shifts are small if compared to those achieved at negative IBPAs.

Figures 13 and 14 show the time histories of the lift and mid-chord moment coefficient oscillations. The time on the x axis is made dimensionless by the reciprocal of the oscillation frequency. Only the last simulated period is displayed. The results achieved for different IBPAs are reported. Significant reductions in the peaks of lift coefficient are found, hence major alleviations of the corresponding vibration could be achieved. The affection of plasma actuation

on the oscillations of moment coefficient is lower compared to the effects on lift. Specifically the plasma-equipped cascade features a light decrease of the moment oscillations for most of the simulated IBPAs. A small increase in the pitching moment amplitude is encountered only at IBPAs of -45, 0 and 45 degrees. It's worth remarking that in Ref. [**?**] we trigger the pressure/suction control according to the moment phase relative to the blade oscillation – rather than according to the sign of the blade motion derivative. This allows for remarkably larger alleviations in the pitching moment oscillations, but much smaller effectiveness on the lift coefficient and on the aeroelastic stability. As a consequence the choice of the control phasing should be done according to the most severe problem – flutter or vibration induced fatigue – occurring under the concurrent operating conditions. In fact the flutter onset is determined by the sign of the area covered by the pitching moment hysteresis curve. On the other hand vibration is related to the amplitude of the hysteresis cycle, that is by the absolute area subtended by the moment curve, rather than on its sign. Therefore large vibratory loads can be encountered also when the blades are far from the instability threshold. On the contrary flutter can occur also when vibratory loads are not particularly large. According to the phasing imposed to the control it is possible to address more effectively either aeroealstic stability or fatigue problems.

5 Conclusions

A numerical assessment of virtual control surfaces for the improvement of the aerostructural response on a compressor cascade is presented. Virtual control surfaces are realized by plasma actuators located both on the pressure and on the suction side at the trailing edge of the blades. The plasma induced flow is conceived to be against the freestream velocity, to generate controlled recirculating flow areas comparable to those achieved with mechanical devices. Simulations at constant angle of attack highlight that pressure side actuation yields effects which are comparable to those of flap-like devices, in terms of flow field, pressure distribution and integral loads. Namely a remarkable lift enhancement along side a light increase in the nose-down pitching moment are achieved. On the contrary suction side actuation provides lift alleviations and reductions in the nose-down pitching moment. No significant drawbacks in terms of drag rises are encountered, both with pressure and with suction side actuation. Traveling wave mode simulations – with the blades oscillating in pitch – are performed to investigate the effects of alternate pressure/suction side actuation on aerodynamic work and vibration. Pressure side actuation is triggered during the downstroke phase of the blade motion. On the other hand suction side actuation is employed during the upstroke phase of the pitching cycle. It is found that actuation provides a remarkable stabilizing effect to the blade aeroelastic response. Namely the flutter instability peak occurring at IBPA = -51.43 deg. is completely withdrawn and the net flux of aerodynamic work is switched to the blade-to-flow direction. Moreover an effective stabilizing effect is encountered for all of the negative IBPAs. For positive IBPAs the clean cascade is already stable, and the effects induced by actuation are very small. Furthermore a beneficial affection of plasma on vibratory loads is observed. The peaks in unsteady lift, responsible of vertical dynamic loads on the cascade, are remarkably reduced. Smaller effects on the oscillations of pitching moment are observed. The present work shows that plasma actuators, employed as virtual control surfaces, could effectively counteract flutter and vibration problems on turbomachines, and may contribute to the solve the feasibility problems of modern thin, highly cambered and heavily loaded blade designs.

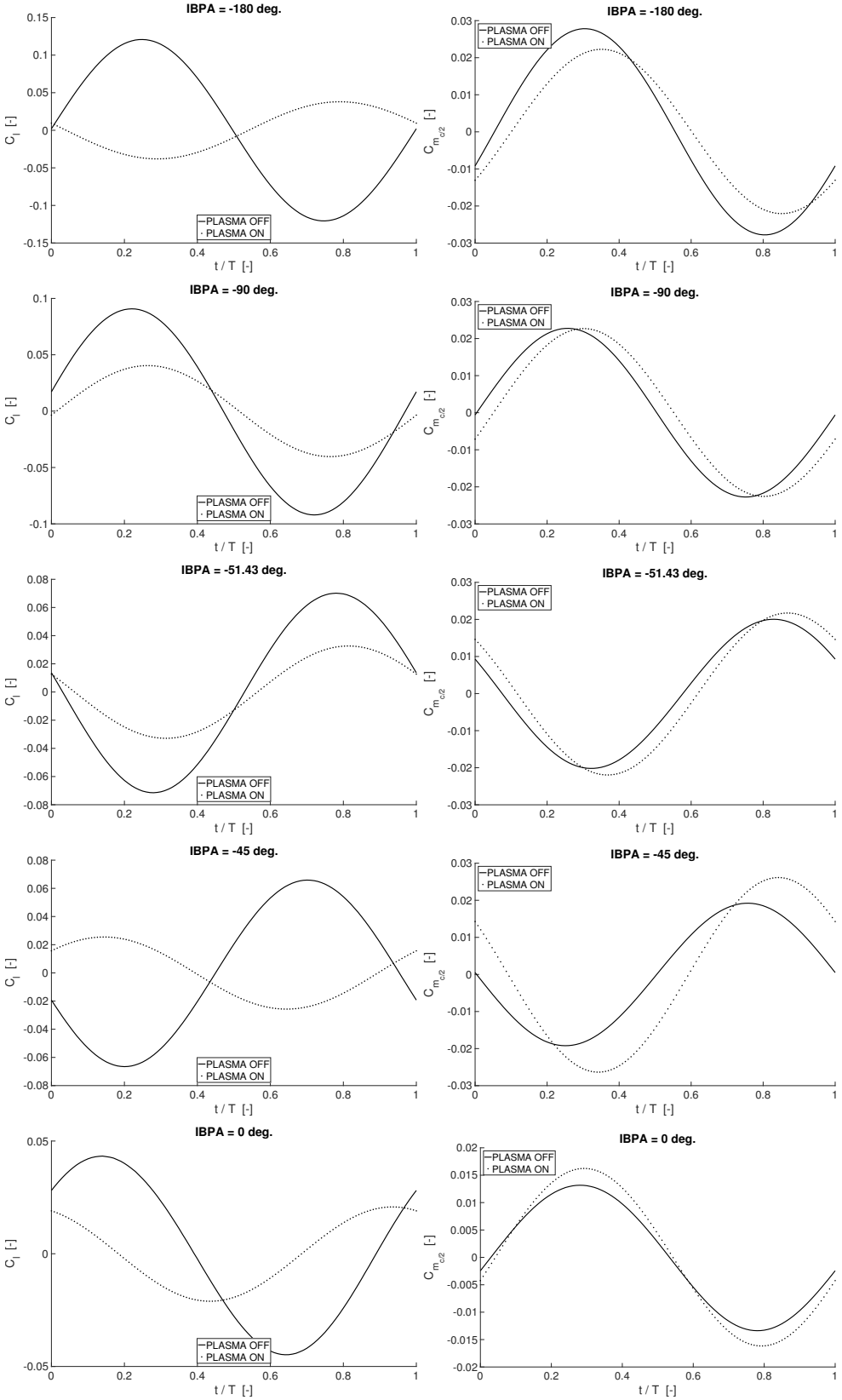

Figure 13: Time history of lift and moment coefficient oscillations without and with actuation; Re ∼195000; IBPA $\in [-180 \quad 0]$ degrees; $\alpha = 2 + \sin 2\pi \mathrm{f}\, \mathrm{t} + \mathrm{IBPA}\pi/180$ degrees; $\mathrm{f} = 19.17$ Hz, $\mathrm{T} = 1/\mathrm{f}$.

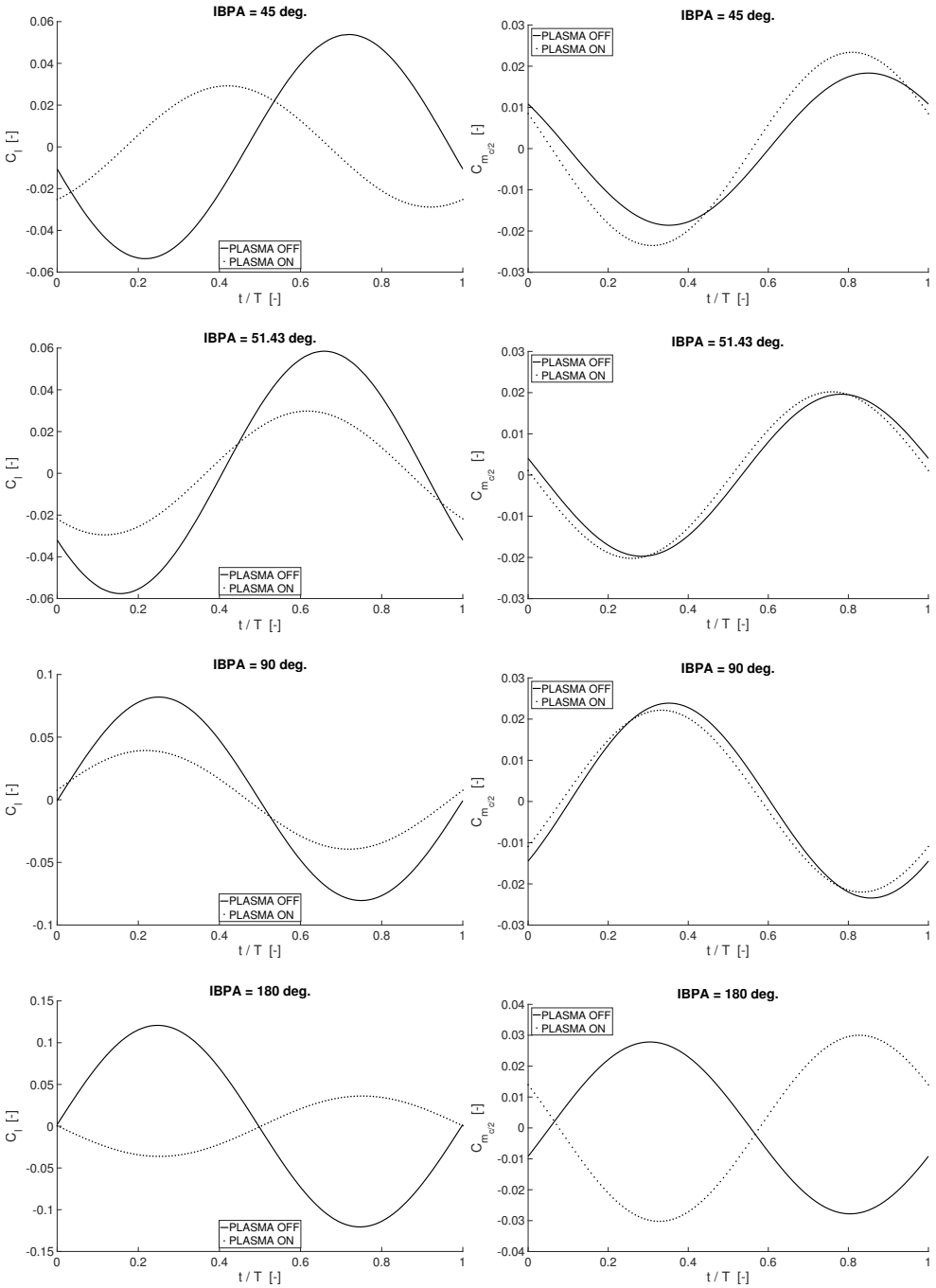

Figure 14: Time history of lift and moment coefficients oscillations without and with actuation; Re $\sim$195000; IBPA $\in [45 \quad 180]$ degrees; $\alpha = 2 + \sin 2\pi \mathrm{f}\, \mathrm{t} + \mathrm{IBPA}\pi/180$ degrees; $\mathrm{f} = 19.17$ Hz, $\mathrm{T} = 1/\mathrm{f}$.

References

[1] Panovski, J. and Kielb, R. E. A Design Method to Prevent Low Pressure Turbine Blade Flutter. In *ASME International Gas Turbine and Aeroengine Congress and Exhibition, 2–5 June 1998, Stockholm, Sweden*, GT-575.

[2] Huang, X. Q. and Bell, D. L. (2006). Influence of upstream stator on rotor flutter stability in a low pressure steam turbine stage. *Proceedings of the Institution of Mechanical Engineers, Part A: Journal of Power and Energy*, 220(2), 23–35.

[3] Tiedemann, C., Heinrich, A., and Peitsch, D. (25—28 June 2012). A New Linear High Speed Compressor Stator Cascade for Active Flow Control Investigations. In *6th AIAA Flow Control Conference*. New Orleans, LA, USA.

[4] Matejka, M., Popelka, L., Safarik, P., et al. (9–13 June 2008). Influence of Active Methods of Flow Control on Compressor Blade Cascade Flow. In *ASME Turbo Expo 2008, Berlin, Germany*, GT2008-51109.

[5] Trávníček, Z., Cyrus, V., Šimurda, D., et al. (2013). Experimental investigation of the compressor cascade under an active flow control. *EPJ Web of Conferences*, 45. doi: http://dx.doi.org/10.1051/epjconf/20134501086.

[6] Hammer, S., Phan, D. T., Peter, J., et al. (10–12 September 2014). Active flow control by adaptive blade systems in periodic unsteady flow conditions. In *Active Flow and Combustion Control*. Berlin, Germany.

[7] Monner, H. P., Huxdorf, O., Riemenschneider, J., et al. (5–9 January 2015). Design and manufacturing of morphing fan blades for experimental investigations in a cascaded wind tunnel. In *23rd AIAA/AHS Adaptive Structures Conference*, AIAA 2015-0790. Kissimmee, FL, USA: American Institute of Aeronautics and Astronautics.

[8] Suman, A., Fortini, A., Aldi, N., et al. (15–19 June 2015). A Shape Memory Alloy-Based Morphing Axial Fan Blade: Part II — Blade Shape and CFD Analyses. In *ASME Turbo Expo 2015: Turbine Technical Conference and Exposition*, GT2015-42700. Montreal, QC, Canada.

[9] Suman, A., Fortini, A., Aldi, N., et al. (15–19 June 2015). A Shape Memory Alloy-Based Morphing Axial Fan Blade: Part I — Blade Structure Design and Functional Characterization. In *ASME Turbo Expo 2015: Turbine Technical Conference and Exposition*, GT2015-42695. Montreal, QC, Canada: American Society of Mechanical Engineers.

[10] Vo, H. D., Cameron, J. D., and Morris, S. C. (2008). Control of Short Length-Scale Rotating Stall Inception on a High-Speed Axial Compressor with Plasma Actuation. In *Proceedings of ASME Turbo Expo 2008: Power for Land, Sea and Air*, GT2008-50967. Berlin, Germany: American Society of Mechanical Engineers.

[11] De Giorgi, M. G., Pescini, E., Marra, F., et al. (16–20 June 2014). Experimental and numerical analysis of a micro plasma actuator for active flow control in turbomachinery. In *Proceedings of ASME Turbo Expo 2014: Turbine Technical Conference and Exposition*, GT2014-25337. Düsseldorf, Germany: American Society of Mechanical Engineers.

[12] Akcayoz, E., Huu, D. V., and Mahallati, A. (2016). Controlling corner stall separation with plasma actuators in a compressor cascade. *Journal of Turbomachinery*, 138(8). doi: 10.1115/1.4032675.

[13] Roget, B. and Chopra, I. Wind-tunnel testing of rotor with individually controlled trailing-edge flaps for vibration reduction. *Journal of Aircraft*, 45(3), 868–879.

[14] Friedmann, P. P., and Millott, T. A. (1995). Vibration Reduction in Rotorcraft Using Active Control: A Comparison of Various Approaches. *Journal of Guidance, Control, and Dynamics*, 18(4), 664–673.

[15] Motta, V., Guardone, A., and Quaranta, G. (24–26 June 2013). Numerical investigation of an L-shaped deployable Gurney flap for rotorcraft vibration control. In *International Forum on Aeroelasticity and Structural Dynamics*. Bristol, UK: Royal Aeronautical Society.

[16] Motta, V. (2015). *Computational fluid dynamic analysis of a L-shaped Gurney flap for vibration control*. Ph.D. thesis, Politecnico di Milano. `http://hdl.handle.net/10589/100350`.

[17] Motta, V. and Quaranta, G. (2015). Linear Reduced-Order Model for Unsteady Aerodynamics of an L-Shaped Gurney Flap. *Journal of Aircraft*, 52, 1887–1904. doi: 10.2514/1.C033099.

[18] Motta, V., Zanotti, A., Gibertini, G., et al. (2016). Numerical assessment of an L-shaped Gurney flap for load control. *Proceedings of the Institution of Mechanical Engineers, Part G: Journal of Aerospace Engineering*, 138. doi:10.1177/0954410016646512.

[19] Motta, V. and Quaranta, G. (2016). A comparative assessment of vibration control capabilities of a L-shaped Gurney flap. *The Aeronautical Journal*, 120(1233), 1812–1831. doi:10.1017/aer.2016.109.

[20] Feng, L., Choi, K., and Wang, J. (2015). Flow control over an airfoil using virtual Gurney flaps. *Journal of Fluid Mechanics*, 767, 595–626.

[21] He, C., Corke, T. C., and Patel, M. P. (2009). Plasma flaps and slats: An application of weakly ionized plasma actuators. *Journal of Aircraft*, 46(3), 864–873.

[22] Malzacher, L., Geist, S., Peitsch, D., et al. (12–16 June 2016). A low speed compressor test rig for flutter investigations. In *Proceedings of ASME Turbo Expo 2016: Turbomachinery Technical Conference and Exposition*, GT2016-57960. Seoul, South Korea.

[23] Carta, F. O. (1982). An Experimental Investigation of Gapwise Periodicity and Unsteady Aerodynamic Response in an Oscillating Cascade. Contractor Report 3523, NASA, United Technologies Research Center.

[24] Zanotti, A., Grassi, D., and Gibertini, G. (2014). Experimental investigation of a trailing edge L-shaped tab on a pitching airfoil in deep dynamic stall conditions. *Proceedings of the Institution of Mechanical Engineers, Part G: Journal of Aerospace Engineering*, 228(12), 2371–2382. doi:10.1177/0954410013517089.

[25] Wang, J., Choi, K., Feng, L., et al. (2013). Recent developments in dbd plasma flow control. *Progress in Aerospace Sciences*, 62, 52–78.

[26] West, T. K. and Hosder, S. (2013). Numerical investigation of plasma actuator configurations for flow separation control at multiple angles of attack. *International Journal of Flow Control*, 5(1).

[27] Aholt, J. and Finaish, F. (4–7 January 2011). Active Flow Control Strategy of Laminar Separation Bubbles Developed over Subsonic Airfoils at Low Reynolds Numbers. In *49th AIAA Aerospace Sciences Meeting including the New Horizons Forum and Aerospace Exposition*, AIAA 2011–733. Orlando, FL, USA.

[28] Ibrahimoglu, B., Yilmazoglu, M. Z., and Cücen, A. (2016). Numerical Analysis of Active Control of Flow on a DBD Plasma Actuator Integrated Airfoil. In *Sustainable Aviation: Energy and Environmental Issues*, chap. 8. Springer International Publishing. ISBN 978-3-319-34181-1, pp. 363–374. doi:10.1007/978-3-319-34181-1_30.

[29] Corke, T. C., Post, M. L., and Orlov, D. M. (2007). SDBD plasma enhanced aerodynamics: concepts, optimization and application. *Progress in Aerospace Sciences*, 43(7–8), 193–217.

[30] Shyy, W., Jayaraman, B., and Andersson, D. Modeling of glow discharge-induced fluid dynamics. *Journal of Applied Physics*, 92(11).

[31] Corke, T. C. and Post, M. L. (10–13 January 2005). Overview of Plasma Flow control: Concepts, Optimization and Applications. In *AIAA-Paper 2005-563, 43rd AIAA Aerospace Sciences Meeting and Exhibit*. Reno, NV, USA: American Institute of Aeronautics and Astronautics.

[32] Abbott, I. and von Doenhoff, A. (1949). *Theory of Wing sections*. New York, NY: Dover Publication, Inc.

[33] Giguère, P., Lemay, J., and Dumas, G. (1995). Gurney flap effects and scaling for low-speed airfoils. In *13th AIAA Applied Aerodynamic Conference*. doi:10.2514/6.1995-1881. AIAA Paper 95-1881-CP.

[34] Hennings, H. (1997). *Flutter investigations on a finite linear 2D compressor cascade in a wind tunnel in incompressible flow*. Ph.D. thesis, RWTH Aachen.

[35] Vasanthakumar, P. (6–10 June 2011). Computation of aerodynamic damping for flutter analysis of a transonic fan. In *ASME 2011 Turbo Expo: Turbine Technical Conference and Exposition*. Vancouver, BC, Canada: American Society of Mechanical Engineers, pp. 1429–1437.

[36] Hennings, H. and Belz, J. (7–10 June 1999). Experimental investigation of the aerodynamic stability of an annular compressor cascade performing tuned pitching oscillations in transonic flow. In *ASME 1999 International Gas Turbine and Aeroengine Congress and Exhibition*. Indianapolis, IN, USA, pp. V004T03A045–V004T03A045.

[37] Watanabe, T. and Kaji, S. (1984). Possibility of cascade flutter suppression by use of non-rigid duct walls. In *The Symposium Proceedings of Unsteady Aerodynamics of Turbomachines and Propellers*. Cambridge, England: Cambridge University, pp. 261–276.

[38] Sun, X. and Kaji, S. (2000). Effects of wall admittance changes on aeroelastic stability of turbomachines. *AIAA journal*, 38(9), 1525–1533.

[39] Sun, X., Jing, X., and Zhao, H. (2001). Control of blade flutter by smart-casing treatment. *Journal of Propulsion and Power*, 17(2), 248–255. doi:10.2514/2.5770.

[40] Leichtfuß, S., Holzinger, F., Brandstetter, C., et al. (3–7 June 2013). Aeroelastic investigation of a transonic research compressor. In *ASME Turbo Expo 2013: Turbine Technical Conference and Exposition*, GT2013-94730. San Antonio, TX, USA: American Society of Mechanical Engineers. doi:10.1115/GT2013-94730.

Copyright statement